ORIGINAL ARTICLE

J Nickel
R Spilker
L Iwasaki
Y Gonzalez
WD McCall
R Ohrbach
MW Beatty
D Marx

Static and dynamic mechanics of the temporomandibular joint: plowing forces, joint load and tissue stress

Authors' affiliations:
J. Nickel, L. Iwasaki, Department of Orthodontics and Dentofacial Orthopedics, and Department of Oral Biology, School of Dentistry, University of Missouri-Kansas City, Kansas City, MO, USA
R. Spilker, Department of Biomedical Engineering, Jonsson Engineering Center, Rensselaer Polytechnic Institute, Rensselaer, NY, USA
Y. Gonzalez, W.D. McCall, R. Ohrbach, Department of Oral Diagnostic Sciences, School of Dental Medicine, University at Buffalo, Buffalo, NY, USA
M.W. Beatty, Departments of Adult Restorative Dentistry and Oral Biology, College of Dentistry, University of Nebraska Medical Center, Lincoln, NE, USA
D. Marx, Department of Statistics, University of Nebraska, Lincoln, NE, USA

Correspondence to:
Jeffrey Nickel
Department of Orthodontics and Dentofacial Orthopedics
University of Missouri-Kansas City School of Dentistry
650 E. 25th St Kansas City
64108 MO
USA
E-mail nickeljc@umkc.edu

Structured Abstract

Authors – Nickel J, Spilker R, Iwasaki L, Gonzalez Y, McCall WD, Ohrbach R, Beatty MW, Marx D

Objectives – To determine the combined effects 1) of stress-field aspect ratio and velocity and compressive strain and 2) joint load, on temporomandibular joint (TMJ) disc mechanics.

Setting and Sample Population – Fifty-two subjects (30 ♀; 22 ♂) participated in the TMJ load experiments.

Material and Methods – In the absence of human tissue, pig TMJ discs were used to determine the effects of variables 1) on surface plowing forces, and to build a biphasic finite element model (bFEM) to test the effect of human joint loads and 2) on tissue stresses. In the laboratory, discs received a 7.6 N static load via an acrylic indenter before cyclic movement. Data were recorded and analysed using ANOVA. To determine human joint loads, Research Diagnostic Criteria calibrated investigators classified subjects based on signs of disc displacement (DD) and pain (+DD/+pain, n = 18; +DD/−pain, n = 17; −DD/−pain, n = 17). Three-dimensional geometries were produced for each subject and used in a computer model to calculate joint loads.

Results – The combined effects of compressive strain, and aspect ratio and velocity of stress-field translation correlated with plowing forces (R^2 = 0.85). +DD/−pain subjects produced 60% higher joint loads (ANOVA, $p < 0.05$), which increased bFEM-calculated compressive strain and peak total normal stress.

Conclusions – Static and dynamic variables of the stress-field and subject-dependent joint load significantly affect disc mechanics.

Key words: biphasic finite element model; cartilage; mechanics; plowing; temporomandibular joint

Dates:
Accepted 15 February 2009

To cite this article:
Nickel J, Spilker R, Iwasaki L, Gonzalez Y, McCall WD, Ohrbach R, Beatty MW, Marx D: Static and dynamic mechanics of the temporomandibular joint: plowing forces, joint load and tissue stress
Orthod Craniofac Res 2009;**12**:159–167

Introduction

Degenerative joint disease (DJD) of the temporomandibular joint (TMJ) is evident in 3–29% of the population aged 19–40 years (1) and shows an age-dependent increase in the severity of tissue disintegration to about age 60 years (2). The mean age of onset of DJD in the TMJ is between 25 and 35 years (1, 3–5), which is over a decade earlier than DJD in the hip (6–8). The variables associated with mechanical failure of the articulating tissues in young synovial joints are rarely investigated (9, 10). Donzelli et al. (11) performed dynamic numerical simulation of the TMJ using physiologically relevant geometry and kinetics derived from a human subject by dynamic stereometry (9, 10). They reported that stress-field translation and subsequent shear strain localization is greatest in the lateral portion of the disc where disc degeneration often occurs (12).

Tractional forces on the surface of the TMJ disc are produced by friction and plowing forces. Stress-field translation and consequential plowing forces (13–15) may contribute to cartilage wear and fatigue, in particular if the translation is mediolateral, because the disc is relatively weak in this aspect (16, 17). Given that the TMJ disc has the function of stress-distribution and lubrication in the TMJ (13–15, 18–20), the mechanical failure of the disc may be an important predisposing factor leading to early DJD.

For the TMJ disc, plowing forces are expected to be the dominant component of tractional forces. This is because laboratory studies have shown that static and, especially, dynamic frictional forces measured on the surface of the TMJ disc are low (13, 18, 21), and tractional forces associated with plowing on the surface of the TMJ disc are 10 times larger (13, 14), and consistent with the tractional forces measured in whole TMJ experiments (22, 23).

It is unknown whether or not inter-individual differences in TMJ loads will also have a significant effect on tissue mechanics. Computer-assisted modelling of the muscle and joint forces in the human craniomandibular system has become an attractive method of studying the control of the mandible during loading. Numerical models based on minimization of joint loads and muscle effort have consistently produced biologically feasible results for static tasks (24–31).

The current project tested the effects of static and dynamic variables associated with loading of the TMJ disc on production of surface tractional forces and tissue stresses. To accomplish this:

1 Laboratory experiments used static and dynamic loading of pig TMJ discs to test the hypothesis that compressive strain, stress-field geometry and velocity of translation influence surface tractional forces.
2 A validated numerical model was used to calculate TMJ loads to test the hypothesis that there were significant differences in TMJ loads amongst humans.
3 A biphasic finite element model (bFEM) was built using the data collected from the TMJ disc experiments, and applied to test the hypothesis that differences in TMJ loads produced significant effects on tissue stress.

Material and methods

Laboratory experiments testing the effects of static and dynamic loading of the pig TMJ disc

Ideally, the study of the effect of loading on TMJ disc mechanics requires non-preserved human specimens. Given the difficulty in procuring and maintaining fresh human tissue, 187 fresh porcine TMJ discs were used. The porcine disc was chosen based on geometric, microstructural and biochemical similarities (32–34).

Temporomandibular joint discs were obtained from a local abattoir in a manner consistent with institutional regulations. Discs were identified and stored separately in 0.1 M phosphate buffered physiological saline solution (PBS, pH = 7.3). During experiments, discs were maintained at 39°C in PBS.

Each disc was tested once employing equipment and methods described previously (13, 14). A load was applied, first statically for 1 (n = 30), 5 (n = 47), 10 (n = 22), 30 (n = 25) or 60 (n = 63) s, and then dynamically along the mediolateral axis of the disc using a hinged beam apparatus (Figs 1A,B and 2A). A normal (perpendicular) load of 7.6 N was imposed on the disc via an acrylic indenter, shaped to produce a mediolateral radius of contact similar to that measured in humans (10). Stress-field translation following static loading was confirmed by fluctuating compressive stresses with respect to time measured by a linear array of nine pressure transducers, 3 mm apart, under the disc (Figs 1B and 2B).

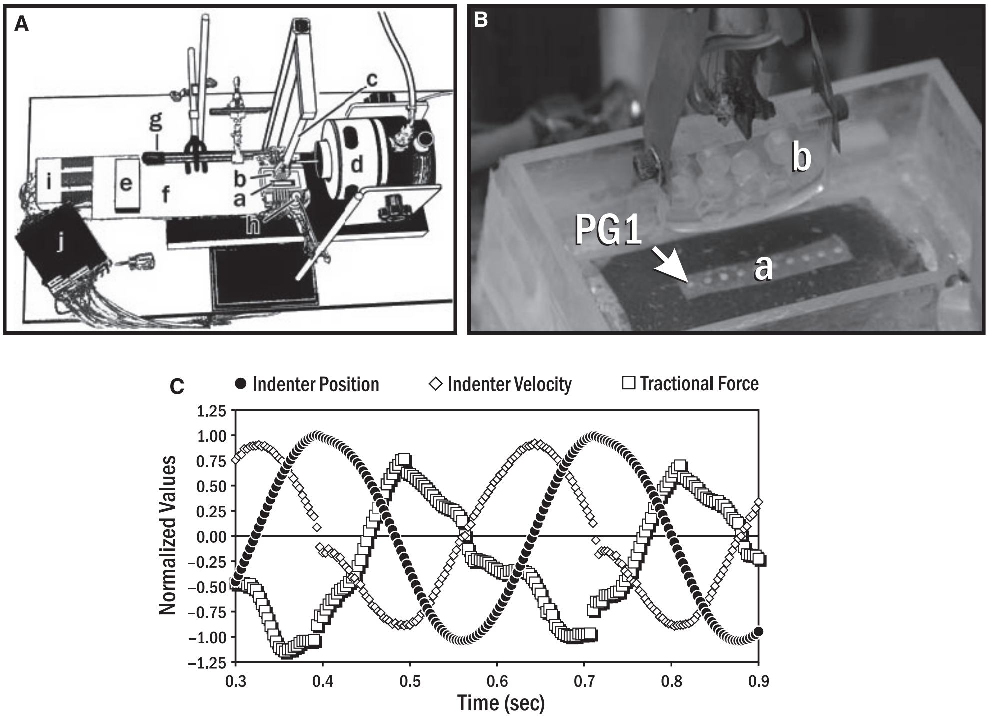

Fig. 1. Plowing equipment and data output [A, B, C; modified from (13)]. (a) Pressure sensitive array: pressure gauge (PG) transducers measured pressure along the mediolateral axis of the disc. (b) Indenter and (c) pendulum arm: the acrylic indenter had polished loading surfaces. An instrumented steel strut measured tractional forces in real-time. (d) Electromagnetic force generator: a computer and custom-built software controlled the position and velocity of force generator displacement. An accelerometer output identified the start of movement. (e) Counter-weight: this mass countered the mass of the loading tray and housing supporting the transducer array. (f) Loading beam: the hinged beam caused the acrylic indenter to load the TMJ disc at the other end of the beam. During experiments, the disc was supported by a curved acrylic base and tray. (g) LVDT used to measure real-time horizontal position of the indenter relative to the disc. (h) LVDT used to measure cartilage thickness. (i) Static load platform: the 7.6 N mass was placed in this position to produce the static loads prior to the start of movement. (j) Power supply/Amplifier box: analogue signals from the pressure transducer array were amplified before digitizing and storing on a 16 channel recorder. Fig. 1C demonstrates real-time recording of indenter position and velocity, and instantaneous measurement of tractional coefficient.

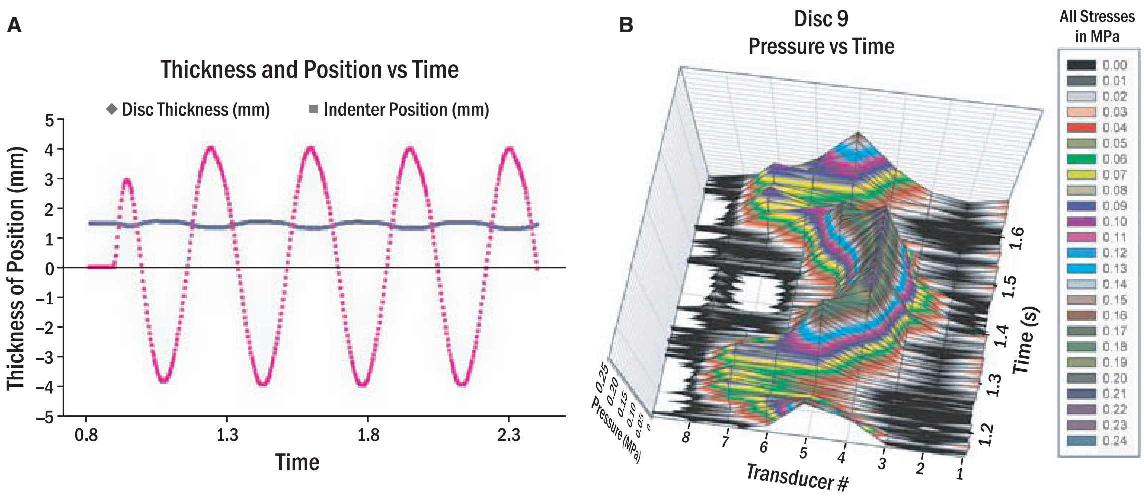

Fig. 2. Indenter movement, disc thickness and stress-field translation. (A) Disc thickness (mm) was continuously measured as the position (mm) of the loaded indenter moved over the surface of the disc. (B) Data from the transducer array recorded the temporospatial changes in total normal stress (MPa) along the mediolateral axis of the disc.

The application of load and the time-dependent changes in compressive strains of the TMJ disc were recorded continuously to within 0.05 mm using a calibrated linear voltage differential transformer (LVDT, Fig. 1A). Following the period of static loading, a computer-controlled electromagnetic force generator was used to move the loaded indenter. Position and velocity of the indenter were determined by calibrated electrical output from a second LVDT (Fig. 1C). Calibration of the instrumented strut permitted measurement of tractional forces to an accuracy of ±0.05 N (Fig. 1B,C).

Determination of inter-individual differences in TMJ loads

Fifty-two subjects (30 ♀ and 22 ♂) at the University of Buffalo gave informed consent to participate. The study was approved by the Institutional Review Boards affiliated with the investigators. Research Diagnostic Criteria (35) calibrated investigators used clinical examination and magnetic resonance imaging (MRI) to classify subjects into three groups: +DD/+pain – subjects with disc displacement (DD) and masticatory muscle pain, +DD/−pain – subjects with DD but free of masticatory muscle pain, and −DD/−pain – healthy subjects. Average age of subjects in the +DD/+pain (n = 18), +DD/−pain (n = 17), and −DD/−pain (n = 17) groups were 37 (range: 21–62), 35 (range: 19–62) and 34 (range: 20–57) years respectively. Using previously described methods (24, 25, 29, 30) the relative positions of the condyles, teeth and five pairs of masticatory muscles (masseter, anterior temporalis, medial pterygoid, lateral pterygoid, anterior digastric) were determined from standardized lateral and postero-anterior cephalometric radiographs, according to a three-dimensional (3D) coordinate system (Fig. 3).

The ability of the numerical model, based on minimization of joint load to predict the morphology TMJ eminence morphology in each subject, was used to test accuracy. The 3D anatomical data were used in the numerical model (31) to predict TMJ eminence morphology.

Three-dimensional numerical modelling was used to predict TMJ forces per unit of bite-force (BF) using an objective function of minimization of muscle effort (MME) based on previous evidence that modelling via this function consistently predicted accurate muscle activation patterns for a variety of bite forces (25–27, 29). The MME model calculated muscle and joint forces for 13 BF angles (Table 1) on the incisor, canine and molar teeth. ANOVA was used to test for differences in TMJ loads between diagnostic groups.

A bFEM of TMJ disc

The plowing experiments were modelled as a sliding contact problem involving a rigid, impermeable indenter and a linear biphasic tissue. The tissue was considered to be biphasic, a mixture of solid and fluid phases that interacted through diffusive body forces (36).

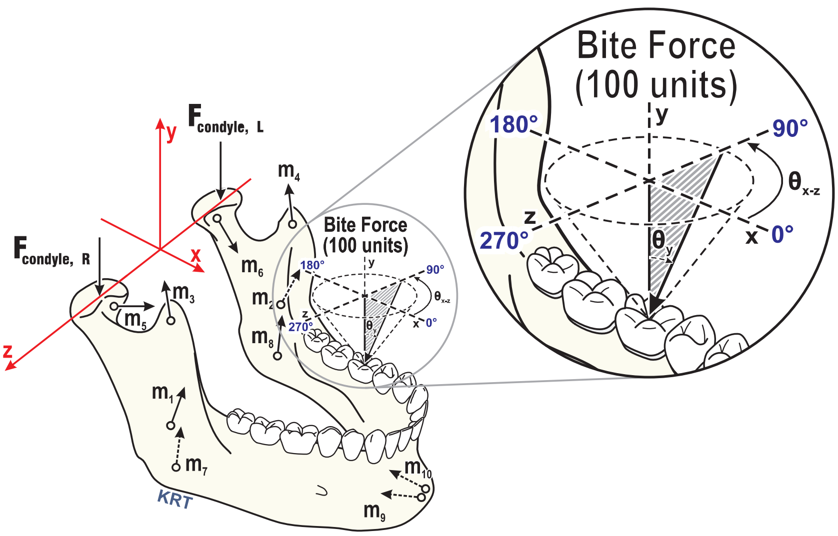

Fig. 3. 3D forces on the mandible (bite-force), joints ($F_{condyle}$), and force vectors of five muscle pairs [$m_{1,2}$ = masseter; $m_{3,4}$ = anterior temporalis; $m_{5,6}$ = lateral pterygoid; $m_{7,8}$ = medial pterygoid; $m_{9,10}$ = anterior digastric muscles; modified from (25, 38)]. The azimuth angle (Θ_{XZ}, °) is parallel to the occlusal plane and varies between 0° and 359°. The vertical angle (Θ_Y, °) describes the angle of the biting-force relative to normal to the occlusal plane (Θ_Y = 0°). Angles within the range of Θ_{XZ} = 270° produced laterally directed loads on the tooth, whereas Θ_{XZ} = 90° produced medially directed loads. Θ_{XZ} = 0° produced posteriorly directed loads, while Θ_{XZ} = 180° produced anteriorly directed loads. The 13 biting-force angles used to test for effects on joint loads (see Table 1).

Table 1. **Definitions of biting angles (see Fig. 3)**

	Bite force direction	
Biting angle	Θ_{XZ}	Θ_Y
1	0	0
2	270	20
3	270	40
4	90	20
5	90	40
6	355	20
7	355	40
8	5	20
9	5	40
10	175	20
11	175	40
12	185	20
13	185	40

The protocol used to conduct the plowing experiments on the TMJ disc resulted in a mixed experiment where, in phase I, the indenter was under static load control for approximately 1 s. As an example, disc 9 (Fig. 2) was modelled such that phase 1 ended at 0.887 s. Phase II followed, where the indenter was moved under displacement control lateromedially in a sinusoidal manner, first to the right, then to the left, resulting in a repeated sinusoidal spatial variation over a period of 0.35 s.

The TMJ disc was modelled two-dimensionally (Fig. 4), with linearly varying thickness of 2.15 mm at the left (medial), 1.7 mm at the right (lateral) and 24 mm in length. The lower surface was supported by a flat, rigid, impermeable surface (no normal flow, no displacement). The left and right boundaries, and the portion of the upper surface outside of the indenter area, were free to displace and for fluid to flow (zero pressure, zero traction). In phase I, the region between points PT1 and PT2 was 13.36 mm long and with mid-point × assumed to be loaded at x = 1 mm by an indenter of 60 mm major radius and 31 mm minor radius of curvature (Fig. 1B). The tissue was indented 19% of original thickness, based on real-time data from the bench-top experiment. The total centred section was 13.36 mm long, centred at x = 1 mm. To simulate the rigid impermeable indenter in the region of PT1–PT2, total normal traction distribution, parabolic in shape, was applied along with the boundary condition of no normal fluid flow. In the biphasic model, this total normal traction was shared between the solid and fluid phases. Phase II modelling involved movement of the indenter over the TMJ disc surface. This was accomplished using Arbitrary Lagrange Eulerian moving mesh capabilities (37) in the latest version (3.4) of COMSOL Multiphysics® (COMSOL, Inc., Burlington, MA, USA) to move the indenter area and corresponding mesh. The biphasic material properties used were Young's modulus (0.0867 MPa) and Poisson's ratio (0.125) of the solid phase, and permeability (7.6×10^{-15} m^4/Ns). The solid content was 17%, and fluid content was 83%.

Results

Variables affecting tractional forces during the start of movement

The combined effects of velocity of stress-field translation, aspect ratio and cube of the compressive strain were found to be correlated with a nonlinear increase in the tractional coefficient ($F_{traction}/F_{normal}$; Fig. 5, R^2 = 0.85).

Variation in human TMJ Loads

Significant inter-group differences in ipsilateral and contralateral TMJ loads were found (Fig. 6A-ipsilateral, B-contralateral), where the +DD/−pain group had

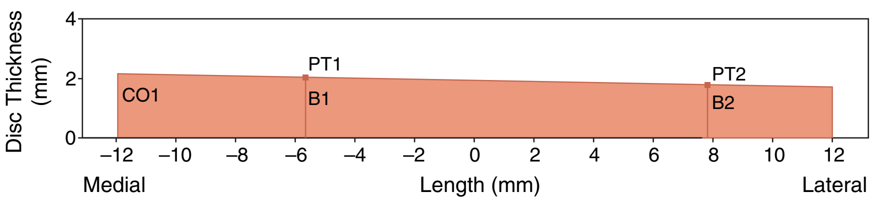

Fig. 4. Two-dimensional geometry of the bFEM (e.g. disc 9). Tissue length was 24 mm, and the tissue thickness changed linearly from 2.15 mm on the left (medial edge, x = −12 mm) to 1.7 mm on the right (lateral edge, x = 12 mm). Points P1 and P2 were located at x = −5.68 and 7.78 mm, respectively, and were the limits of the applied contact traction. This region of contact length was 13.36 mm, and was centred at x = 1 mm. The quadrilateral mesh had 2935 elements and 61 799 degrees of freedom. Horizonatal axis – mediolateral position (mm). Vertical axis – disc thickness (mm).

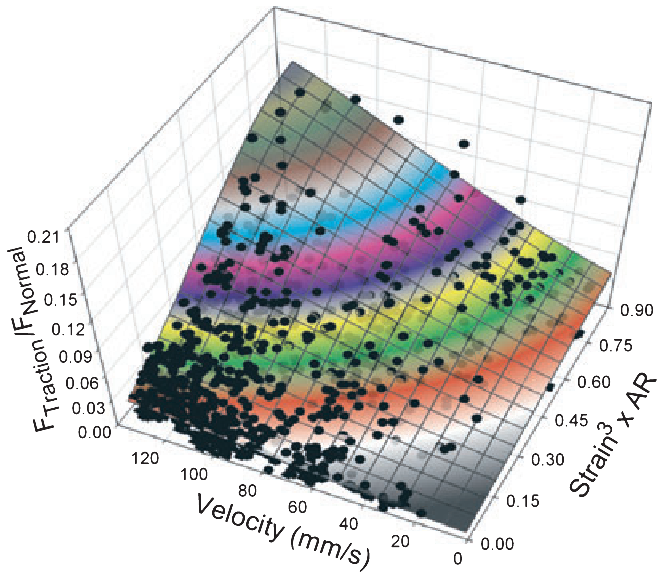

Fig. 5. Effect of strain, aspect ratio, velocity of translation on tractional forces. The regression equation form is: $f = a^{(-0.5(((x-x_0)/b)^2+((y-y_0)/c)^2))}$, with constants a = 0.18; b = 0.52 and c = 106 (mm/s). Variables were tractional coefficient, velocity of movement (Y_0 = 183 mm/s), and the product of aspect ratio and the cube of the compressive strain (X_0 = 0.91). The combined effects of the variables correlated with a non-linear increase in the tractional coefficient ($F_{\text{traction}}/F_{\text{normal}}$; R^2 = 0.85).

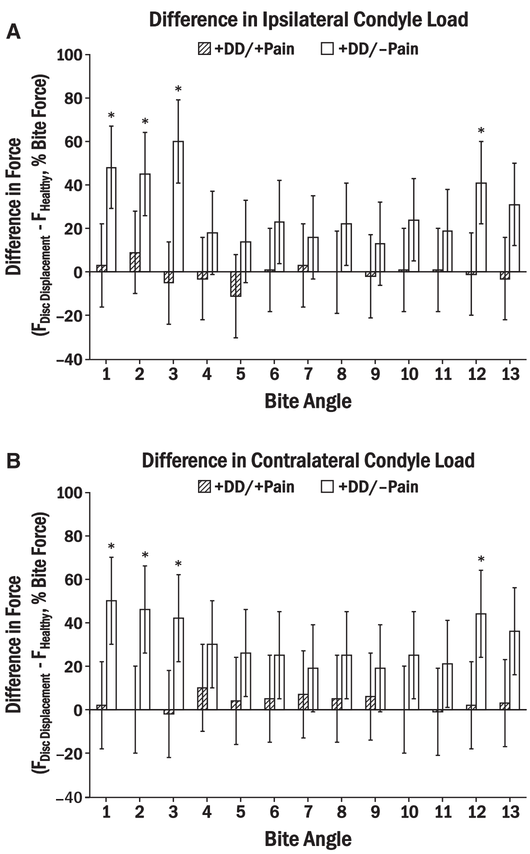

Fig. 6. The effect of biting angle on differences in condyle loads: Biting angles 1–13 (horizontal axis) are defined in Table 1. Difference in TMJ load between the +DD/–pain group or +DD/+pain group and –DD/–pain are plotted on the vertical axis. (A) Ipsilateral and (B) contralateral differences are shown. The '*' indicates ANOVA calculated $p < 0.05$.

higher ipsilateral and contralateral joint loads for biting angles 1,2,3 and 12 (all $p < 0.05$).

bFE modelling of load and TMJ disc stress

As part of bFEM validation, calculated temporospatial changes in total normal stresses at the inferior surface of the disc (y = 0, Fig. 4) during phase 1 of static load (t = 0–0.887 s, Fig. 7A), were compared to the experimental data (Fig. 7B). Specifically, experimental and bFEM total normal stresses from pressure gauges 4, 5, and 6 were compared. bFEM and experimental peak total normal stresses were within ±20%, indicating acceptable model accuracy. In response to a 7.6 N load, Fig. 8A shows bFEM-calculated total normal stresses

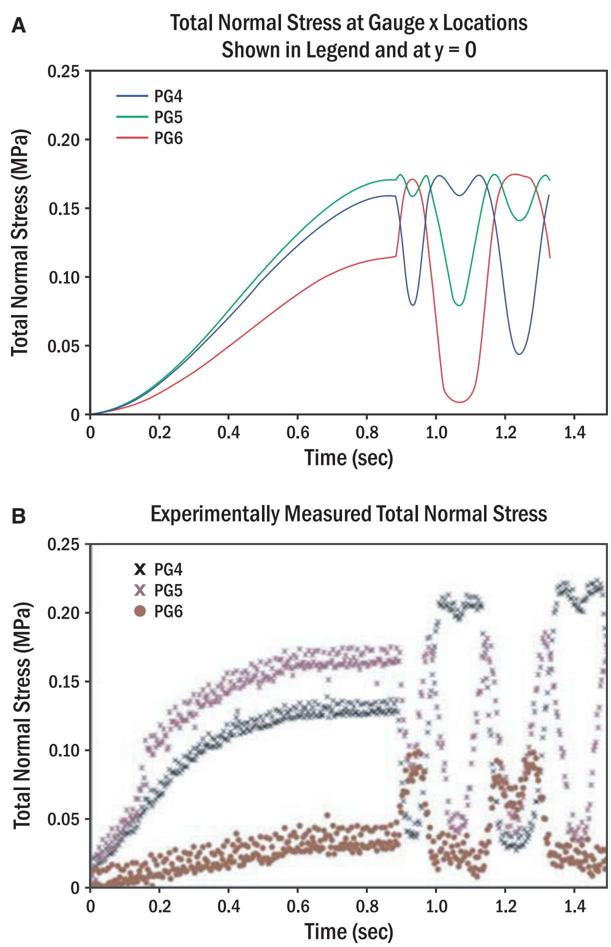

Fig. 7. Tests of bFEM accuracy: (A) bFEM-calculated time-dependent response of the total normal stress (MPa) to 7.6 N load. The stress is the result of solid and fluid phase contributions. The stresses were calculated for positions x = –1, 2 and 3 mm on the disc inferior surface (y = 0). These locations correspond to pressure gauges #4, 5 and 6 (Fig. 7B, MPa). Experimental data from these gauges showed that bFEM accuracy of peak stresses was ±20%. Horizontal axis – time (s). Vertical axis – Total Normal Stress (MPa).

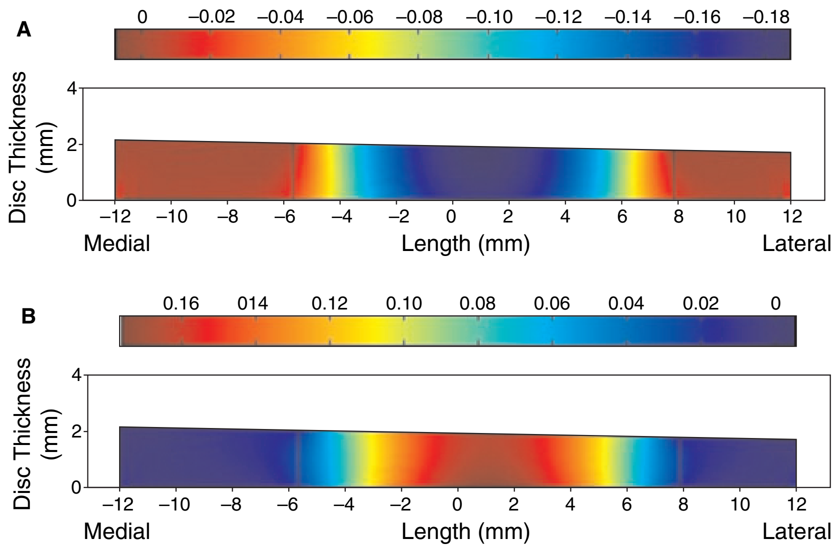

Fig. 8. bFEM-calculated stresses in response to a 7.6 N load: (A) shows the distribution of total normal stress (MPa) at the end of phase I ($t = 0.887$ s). Total normal stress included both solid and fluid phase contributions, with peak values of 0.187 MPa. (B) Shows pressure (MPa) from the fluid phase alone, with peak values of 0.176 MPa. Horizontal axis – mediolateral position (mm). Vertical axis – disc thickness (mm).

(MPa) at the end of phase I ($t = 0.887$ s). Total normal stress includes both solid and fluid phase contributions. Figure 8B shows pressure from the fluid phase alone, demonstrating the overwhelming significance of the fluid phase in the support of a 7.6 N load (Fig. 8A,B). Peak fluid pressures of 0.176 MPa (Fig. 8B) represented 94% of the 0.187 MPa peak normal stress (Fig. 8A).

In accordance with joint load data, a 60% increase in load (12.2 N) increased total normal stresses (7.6 N, Fig. 8A; 12.2 N, Fig. 9) and compressive strain (28% for 10 N, 45% for 16 N) by 1.6 times at the end of phase I.

Discussion

The likelihood of fatigue failure of biomaterials, such as the TMJ disc, depends on the magnitude and frequency of applied stress. During daily activities, +DD/−pain subjects were capable of producing total normal stresses 1.6 times higher than healthy subjects. The data also showed that there were no significant differences in loads between +DD/+pain and −DD/−pain groups. It is possible that load distribution over the surfaces of discs in +DD/+pain subjects produced stress-field geometries and compressive strains which increased tractional (plowing) forces, and thus promoted disc failure. Also possible are differences in frequency of loading between +DD/+pain and −DD/−pain groups, where more frequent application of TMJ loads would fatigue the disc and contribute to the development of myofascial pain. Future work should focus on differences in biobehaviour and intracapsular mechanics in subjects.

Data recorded from the experiments on TMJ discs showed the nonlinear relationship between the variables and tractional forces. The term tractional coefficient was used in this study because the tractional forces measured were the sum of classical frictional and plowing forces on the disc surface. The results of the bFEM calculations showed that the fluid phase carried 94% of the total normal stress. Future work in this area will focus on validation of bFEM during phase II loading of the disc, and the circumstances under

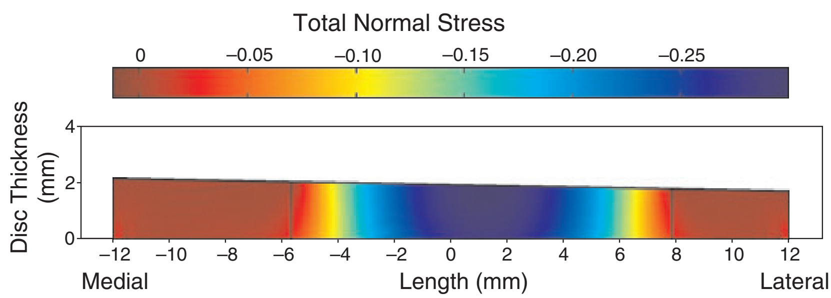

Fig. 9. bFEM distribution of total normal stress (MPa) following the application of a 12.2 N load. The data presented occurred at the end of phase I ($t = 0.887$ s). Compared to data calculated for a 7.6 N, total normal stresses increased to 0.299 MPa. Horizontal axis – mediolateral position (mm). Vertical axis – disc thickness (mm).

which there is transfer of stresses from the fluid to the solid components of the TMJ disc. It is under these circumstances that mechanical fatigue of the disc is promoted.

Conclusions

Inter-group differences in joint load, together with parameters, such as compressive strain produced during a static period of loading, geometry of the stress-field and velocity of translation, are likely to significantly increase tissue stresses and increase the risk of mechanical fatigue of the TMJ disc.

Clinical relevance

Several factors are likely to determine the longevity of the TMJ disc, which is the primary stress-reduction mechanism of the joint. The data presented shows that subjects with TMJ displacement (+DD), but free of myofascial pain (−pain) produce very large TMJ loads. The distribution of loads over the articulating surfaces produces plowing forces which are likely to cause mechanical fatigue of the tissue.

Acknowledgements: This work was supported in part by NIDCR 5R01 DE16417-2 (Nickel, PI). The authors wish to thank the subjects who participated in this project. The authors gratefully acknowledge the contributions of Mike Crosby, Aaron Jacobsen, Krista Evans, Adam Shaver, Laura Rothe, Tien Nguyen, Matthew Moss and Paul Robinson. Mr Bobby Simetich, Biomaterials Laboratory, UNMC College of Dentistry, helped in the collection of the TMJ discs. The authors thank Farmland Foods Corporation, Crete, Nebraska, for their support. Mr Kim Theesen helped to create the illustrations.

References

1. Pullinger AG, Seligman DA, Solberg WK. Temporomandibular disorders. Part I: Functional status, dentomorphologic features, and sex differences in a nonpatient population. *J Prosthet Dent* 1988;59:228–35.
2. Luder HU. Factors affecting degeneration in human temporomandibular joints as assessed histologically. *J Oral Sci* 2002;110:106–13.
3. Heloe B, Heloe LA. Characteristics of a group of patients with temporomandibular joint disorders. *Community Dent Oral Epidemiol* 1975;3:72–9.
4. Nilner M. Prevalence of functional disturbances and diseases of the stomatognathic system in 15–18 year olds. *Swed Dent J* 1981;5:189–97.
5. Solberg WK, Woo MW, Houston JB. Prevalence of mandibular dysfunction in young adults. *J Am Dent Assoc (1939)* 1979;98: 25–34.
6. Felson DT, Zhang Y, Hannan MT, Naimark A, Weissman B, Aliabadi P et al. Risk factors for incident radiographic knee osteoarthritis in the elderly: the Framingham Study. *Arthritis Rheum* 1997;40:728–33.
7. Lawrence RC, Hochberg MC, Kelsey JL, McDuffie FC, Medsger TA Jr, Felts WR et al. Estimates of the prevalence of selected arthritic and musculoskeletal diseases in the United States. *J Rheumatol* 1989;16:427–41.
8. Vingard E, Alfredsson L, Malchau H. Osteoarthrosis of the hip in women and its relation to physical load at work and in the home. *Ann Rheum Dis* 1997;56:293–8.
9. Gallo LM, Brasi M, Ernst B, Palla S. Relevance of mandibular helical axis analysis in functional and dysfunctional TMJs. *J Biomech* 2006;39:1716–25.
10. Gallo LM, Nickel JC, Iwasaki LR, Palla S. Stress-field translation in the healthy human temporomandibular joint. *J Dent Res* 2000;79:1740–6.
11. Donzelli PS, Gallo LM, Spilker RL, Palla S. Biphasic finite element simulation of the TMJ disc from in vivo kinematic and geometric measurements. *J Biomech* 2004;37:1787–91.
12. Oberg T, Carlsson GE, Fajers CM. The temporomandibular joint. A morphologic study on a human autopsy material. *Acta Odontol Scand* 1971;29:349–84.
13. Nickel JC, Iwasaki LR, Beatty MW, Marx DB. Laboratory stresses and tractional forces on the TMJ disc surface. *J Dent Res* 2004;83:650–4.
14. Nickel JC, Iwasaki LR, Beatty MW, Moss MA, Marx DB. Static and dynamic loading effects on temporomandibular joint disc tractional forces. *J Dent Res* 2006;85:809–13.
15. Nickel JC, Iwasaki LR, Gallo LM, Palla S, Marx DB. Tractional forces, work, and energy densities in the human TMJ. In: McNamara JA, editor. *Temporomandibular Disorders and Orofacial Pain*. Ann Arbor, MI: Needham Press; 2009, pp. 427–50.
16. Beatty MW, Bruno MJ, Iwasaki LR, Nickel JC. Strain rate dependent orthotropic properties of pristine and impulsively loaded porcine temporomandibular joint disk. *J Biomed Mater Res* 2001;57:25–34.
17. Beatty MW, Nickel JC, Iwasaki LR, Leiker M. Mechanical response of the porcine temporomandibular joint disc to an impact event and repeated tensile loading. *J Orofac Pain* 2003;17:160–6.
18. Nickel JC, Iwasaki LR, Feely DE, Stormberg KD, Beatty MW. The effect of disc thickness and trauma on disc surface friction in the porcine temporomandibular joint. *Arch Oral Biol* 2001;46:155–62.
19. Nickel JC, McLachlan KR. In vitro measurement of the stress-distribution properties of the pig temporomandibular joint disc. *Arch Oral Biol* 1994;39:439–48.
20. Nickel JC, McLachlan KR. An analysis of surface congruity in the growing human temporomandibular joint. *Arch Oral Biol* 1994;39:315–21.
21. Nickel JC, McLachlan KR. In vitro measurement of the frictional properties of the temporomandibular joint disc. *Arch Oral Biol* 1994;39:323–31.
22. Kawai N, Tanaka E, Takata T, Miyauchi M, Tanaka M, Todoh M et al. Influence of additive hyaluronic acid on the lubricating

ability in the temporomandibular joint. *J Biomed Mater Res A* 2004;70:149–53.

23. Tanaka E, Kawai N, Tanaka M, Todoh M, van Eijden T, Hanaoka K et al. The frictional coefficient of the temporomandibular joint and its dependency on the magnitude and duration of joint loading. *J Dent Res* 2004;83:404–7.
24. Iwasaki LR, Baird BW, McCall WD Jr, Nickel JC. Muscle and temporomandibular joint forces associated with chincup loading predicted by numerical modeling. *Am J Orthod Dentofacial Orthop* 2003;124:530–40.
25. Iwasaki LR, Petsche PE, McCall WD Jr, Marx D, Nickel JC. Neuromuscular objectives of the human masticatory apparatus during static biting. *Arch Oral Biol* 2003;48:767–77.
26. Iwasaki LR, Thornton BR, McCall WD Jr, Nickel JC. Individual variations in numerically modeled human muscle and temporomandibular joint forces during static biting. *J Orofac Pain* 2004;18:235–45.
27. Iwasaki LR, Uchida S, Marx DB, Yotsui Y, Maeda T, Inoue H et al. Ipsilateral and contralateral human TMJ loads compared via validated numerical models. In: McNamara JA, editor. *Temporomandibular Disorders and Orofacial Pain*. Ann Arbor, MI: Needham Press; 2009, pp. 405–25.
28. Nickel JC, Iwasaki LR. In vivo tests of TMJ morphology and masticatory muscle forces predicted by computer-assisted models. In: Davidovitch Z, Mah J, editors. *Biological Mechanisms of Tooth Movement and Craniofacial Adaptation*. Boston, MA: Harvard Society for the Advancement of Orthodontics; 2004. pp. 59–70.
29. Nickel JC, Iwasaki LR, Walker RD, McLachlan KR, McCall WD Jr. Human masticatory muscle forces during static biting. *J Dent Res* 2003;82:212–7.
30. Nickel JC, Yao P, Spalding PM, Iwasaki LR. Validated numerical modeling of the effects of combined orthodontic and orthognathic surgical treatment on TMJ loads and muscle forces. *Am J Orthod Dentofacial Orthop* 2002;121:73–83.
31. Trainor PG, McLachlan KR, McCall WD. Modelling of forces in the human masticatory system with optimization of the angulations of the joint loads. *J Biomech* 1995;28:829–43.
32. Herring SW. The dynamics of mastication in pigs. *Arch Oral Biol* 1976;21:473–80.
33. Strom D, Holm S, Clemensson E, Haraldson T, Carlsson GE. Gross anatomy of the mandibular joint and masticatory muscles in the domestic pig (*Sus scrofa*). *Arch Oral Biol* 1986;31:763–8.
34. Sun Z, Liu ZJ, Herring SW. Movement of temporomandibular joint tissues during mastication and passive manipulation in miniature pigs. *Arch Oral Biol* 2002;47:293–305.
35. Dworkin SF, LeResche L. Research diagnostic criteria for temporomandibular disorders: review, criteria, examinations and specifications, critique. *J Craniomandib Disord* 1992;6:301–55.
36. Mow VC, Kuei SC, Lai WM, Armstrong CG. Biphasic creep and stress relaxation of articular cartilage in compression? Theory and experiments. *J Biomech Eng* 1980;102:73–84.
37. Donéa J, Ponthot J-P, Rodríguez-Ferran A, Huerta A. Arbitrary Lagrangian–Eulerian methods. In: Stein E, De Borst R, Hughes TJR, editors. *Encylopedia of Computational Mechanics*. Hoboken, NJ: Wiley; 2004, pp. 1–25.
38. Smith DM, McLachlan KR, McCall WD Jr. A numerical model of temporomandibular joint loading. *J Dent Res* 1986;65:1046–52.